# A Polar Scaling Technique for the Regularization of Strongly Singular and Strongly Near-Singular Helmholtz Surface Integrals Evaluated over Planar Domains

Brian J. Vaughn

***Abstract*—The numerical integration of expressions containing strong singularities or strong near-singularities has long been a challenging problem in the electromagnetics community. Much attention has been paid to this problem, as strong $1/R^2$ singularities routinely appear when implementing electromagnetic simulation techniques like the Method of Moments (MoM). To date, several techniques, from singularity extraction to singularity cancellation, have been employed to deal with problems of this type. However, no single technique has been proposed that can deal with both strong singularities and strong near-singularities in a fully-numerical manner. Moreover, it has been claimed that the Helmholtz-type strongly singular integral found in the MoM is convergent in a principal value sense, but this has yet to be proven rigorously. In this work, we will conduct the convergence proof and introduce a "polar scaling" change of variables method that may be used to evaluate Helmholtz integrals with both strong and weak singularities/near-singularities. The technique is fully-numerical and can in principle be applied to any planar polygon and any basis function. We will also provide numerical results showing useful convergence behavior for integrals involving both exact and near-singularities.**

***Index Terms*—Integral Equations, Method of Moments, Numerical Simulation.**

## I. Introduction

IT is well known that the method of moments (MoM) technique, a popular method for solving electromagnetic integral equations, requires the numerical evaluation of several integrals containing the Green's Function of the inhomogeneous electromagnetic Helmholtz Equation. This Green's function is represented as:

$$G(\vec{x}, \vec{x'}) = \frac{e^{-jkR}}{4\pi R}, \qquad (1.1)$$

*This manuscript has been authored by Fermi Research Alliance, LLC under Contract No. DE-AC02-07CH11359 with the U.S. Department of Energy, Office of Science, Office of High Energy Physics.*

B. J. Vaughn is with Fermi National Accelerator Laboratory, Batavia, IL, 60510, USA (e-mail: bvaughn@fnal.gov).

where $k$ is the wavenumber and

$$R = \sqrt{(x-x')^2 + (y-y')^2 + (z-z')^2}, \qquad (1.2)$$

where the primed coordinates denote the position of an electromagnetic current source and the unprimed coordinates denote the observation point. Since the field solution is often desired everywhere within a computational domain, computation for values of $R$ approaching 0 are necessary, leading to the task of evaluating integrals with integrands that contain singularities. One such integral that is often invoked is the following surface integral:

$$\nabla \times \int \vec{\boldsymbol{N}}(\vec{x}') \frac{e^{-jkR}}{4\pi R} dS' = \int \frac{-\vec{R} e^{-jkR}(1+jkR)}{4\pi R^3} \times \vec{\boldsymbol{N}}(\vec{x}')\, dS', \qquad (1.3)$$

where $\vec{\boldsymbol{N}}(\vec{x}')$ is a basis function used to approximate a portion of the current source over the surface and $\vec{R}$ is $\vec{x} - \vec{x'}$. Other integrals are involved in the MoM process, but this one is of particular interest, as it contains what is termed a "strong" singularity, i.e., a $1/R^2$ singularity. This type of integral is often treated with the singularity extraction technique, which divides the integral into two, one regular and one singular, and solves the new singular integral analytically [1]-[2]. While powerful and common, this technique is limited in that the analytical integral is not general, and a new formulation must be developed for differing integration domains or basis functions. An equally accurate technique that is more versatile without creating substantially more computational work would therefore have greater utility. Another technique that has been used to treat Helmholtz integral singularities is the singularity cancellation technique, where the integrand is transformed with a change of variables into an expression that no longer contains the singularity, as it is cancelled with the Jacobian [2]-[8]. However, the strong singularity resists cancellation with this method alone and in fact, to the author's knowledge, cancellation schemes have only been achieved for the above type of integral (with a strong singularity) when it is near-singular, not exactly singular, as the transformations detailed

in the works above show diverging or undefined integral limits when the singular point is exactly within the integration source domain. However, several of the near-singularity papers, namely [4] and [5], imply or claim that the exact singularity case is tractable, as the integrand converges to a principal value, and that only the near-singular case is especially challenging. While this claim will be shown to be true in this work, a rigorous proof of the claim does not appear to have been presented in the literature before now; the reference that is often used to support the claim, [3], is a referral to a conference presentation, for which only the abstract is readily available, meaning that it is unclear exactly how the authors drew the convergence conclusion, as it can be made apparent both mathematically with a rigorous proof or empirically with numerical testing. If the latter method was used to draw the conclusion, this would constitute an incomplete justification of the claim. As such, there is a gap in the development of the theory that will be remedied here. It should be noted that the technique detailed in a recent work, [9], treats both near and exact singularities under the same umbrella by combining singularity extraction with singularity cancellation, but this is subject to the same analytical result limitation as the singularity extraction method alone.

Furthermore, the author has identified an opportunity to extend the integration of eqn. (1.3) to planar polygons with an arbitrary number of edges with one universal standard procedure. A formulation that treats all shapes of this type with the same sequence of variable transformations, regardless of basis function and shape type, presents substantial utility to any platform designed with generality in mind. Using this as a motivation, we will develop a general polar transformation (termed "polar scaling"), rigorously prove that it regularizes the integral in eqn. (1.3), and then connect it to an N-sided planar polygon. We will also detail how the method can be applied to near-singularities, creating an all-in-one solution for the type of surface integration considered here. The paper will be organized as follows: Section II. will detail the general polar regularization, Section III. will discuss an equally general coordinate renormalization procedure, Section IV. will describe how to complete the polar transformation once a particular shape is chosen, Section V. will discuss near-singularity treatment, and Section VI. will demonstrate a numerical example.

## II. Polar Regularization

As alluded to in Section I, the polar transformation that will be executed below does not cancel the strong singularity in the conventional manner. However, it will be shown that the transformation used here will result in an integrand that is finite at all points within the integration domain, including the strong singularity. That is, the transformed integrand will have a limit that exists as the observation point approaches the source point. We will now formulate this transformation.

Without loss of generality, for a two-dimensional domain described in $(u, v)$ coordinates, let us define the following transformation to polar coordinates:

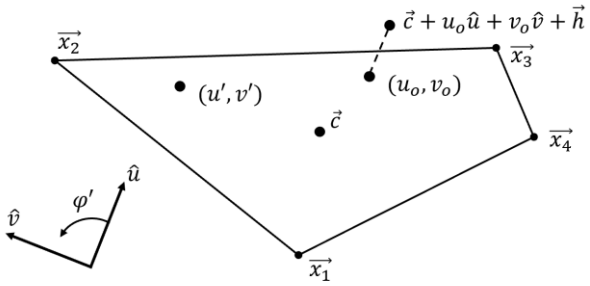


Fig. 1. Arbitrary polygon described in $(u, v)$ coordinate system.

$$u = \rho f(\varphi) + u_0, \tag{2.1a}$$

$$v = \rho f(\varphi)\tan\varphi + v_0, \tag{2.1b}$$

with

$$\vec{x} = \vec{c} + u\hat{u} + v\hat{v} + \vec{h}, \tag{2.1c}$$

$$\overrightarrow{x'} = \vec{c} + u'\hat{u} + v'\hat{v}\,, \tag{2.1d}$$

where $f(\varphi)$ is some angular function yet to be defined, $\vec{c}$ is the source domain centroid, and $(u_0, v_0)$ is the position of the observation point if it is within the source domain, or the projection of the observation point onto the source domain if the observation point is not within the source domain. $\vec{h}$ applies to the case where the observation point is not within the source domain and represents the vector between the observation point and its source domain projection ($\vec{h}$ is merely the 0 vector if the observation point lies within the source domain). $|\vec{h}|$ is the shortest distance between the observation point and any point in the source domain. Note that $\rho$ is real and $\rho \geq 0$. $\hat{u}$ and $\hat{v}$ are orthogonal $(u, v)$-space unit vectors defined according to the shape under consideration, also to be discussed in Section IV. Fig. 1 illustrates this coordinate system, but $\rho$ is omitted as its calculation will be discussed in Section IV; we do not need its formal definition to show regularization. The Jacobian for the change of variables from the $(u, v)$ domain to the $(\rho, \varphi)$ domain is

$$\left|J_{\rho\varphi}\right| = \rho f(\varphi)^2 \sec^2\varphi\,. \tag{2.2}$$

We may substitute these transformations into our expression for $R$, resulting in the following:

$$R = \sqrt{\sum_{n}^{x,y,z} \left\{ \begin{matrix} \widehat{u_n}\left(\rho f(\varphi) - \rho' f(\varphi')\right) \\ +\widehat{v_n}\left(\rho f(\varphi)\tan\varphi - \rho' f(\varphi')\tan\varphi'\right) + h\widehat{h_n} \end{matrix} \right\}^2}\,. \tag{2.3}$$

We stipulate that $(u_0, v_0)$ is the transformed observation point or projection, so $\rho$ is 0. As such, eqn. (2.3) becomes

$$R = \sqrt{\sum_{n}^{x,y,z}\left(\widehat{u_n}\rho' f(\varphi') + \widehat{v_n}\,\rho' f(\varphi')\tan\varphi' - h\widehat{h_n}\right)^2}, \quad (2.4)$$

where $h = |\vec{h}|$ and $\hat{h}$ is the unit vector in the direction of $\vec{h}$. Note that we factored out -1 to reorient the signs in the expression. Let us now use the transformations executed thus far to manipulate the strongly singular Helmholtz integral described in eqn. (1.3):

$$\int \frac{-\vec{R}e^{-jkR}(1+jkR)}{4\pi R^3} \times \vec{N}(\vec{x}')\, dS' = \int \frac{-e^{-jkR}(1+jkR)}{4\pi R^3} * \begin{Bmatrix} (x-x')\left(N_y(\vec{x}')\hat{z} - N_z(\vec{x}')\hat{y}\right) \\ +(y-y')(N_z(\vec{x}')\hat{x} - N_x(\vec{x}')\hat{z}) \\ +(z-z')\left(N_x(\vec{x}')\hat{y} - N_y(\vec{x}')\hat{x}\right) \end{Bmatrix} dS' \quad (2.5)$$

Let us consider only the first term in the brackets for now, leading to the following integral:

$$\int \frac{-e^{-jkR}(1+jkR)}{4\pi R^3}\{(x-x')\left(N_y(\vec{x}')\hat{z} - N_z(\vec{x}')\hat{y}\right)\}dS' \quad (2.6)$$

Further, let

$$N_{yz} \equiv \left(N_y(\vec{x}')\hat{z} - N_z(\vec{x}')\hat{y}\right) \quad (2.7)$$

Substituting the coordinate transformations into eqn. (2.6), we obtain

$$\int \frac{-e^{-jkR}(1+jkR)}{4\pi R^3}\{(x-x')\left(N_y(\vec{x}')\hat{z} - N_z(\vec{x}')\hat{y}\right)\}dS'$$

$$= \int\int \frac{-e^{-jkR}(1+jkR)}{4\pi R^3}\{[\widehat{u_x}(u-u') + \widehat{v_x}(v-v') + h\widehat{h_x}] * N_{yz}(\rho',\varphi')\}\left|J_{\rho'\varphi'}\right| d\rho' d\varphi'$$

$$= \int\int \frac{e^{-jkR}(1+jkR)}{4\pi R^3} * \{\left[\widehat{u_x}\rho' f(\varphi') + \widehat{v_x}\rho' f(\varphi')\tan\varphi' - h\widehat{h_x}\right]N_{yz}(\rho',\varphi')\} * \rho' f(\varphi')^2 \sec^2\varphi'\, d\rho' d\varphi' \quad (2.8)$$

Note that the negative sign in front of the exponential was absorbed into the expression in the square brackets. Also note that the $\rho'$ bounds are 0 and 1, whereas the $\varphi'$ bounds are 0 and $2\pi$. These details will be more closely described later on when we specify the computation of $\rho$ and $f(\varphi)$. Substituting eqn. (2.4) into eqn. (2.8) and splitting the expression into two integrals, we arrive at the following result:

$$\int\int \frac{e^{-jk\sqrt{\sum_n^{x,y,z}\left(\widehat{u_n}\rho' f(\varphi') + \widehat{v_n}\,\rho' f(\varphi')\tan\varphi' - h\widehat{h_n}\right)^2}}}{4\pi\left[\sqrt{\sum_n^{x,y,z}\left(\widehat{u_n}\rho' f(\varphi') + \widehat{v_n}\,\rho' f(\varphi')\tan\varphi' - h\widehat{h_n}\right)^2}\right]^{\frac{3}{2}}} * \begin{bmatrix} \widehat{u_x}\rho' f(\varphi') \\ +\widehat{v_x}\,\rho' f(\varphi')\tan\varphi' \\ -h\widehat{h_x} \end{bmatrix} N_{yz}(\rho',\varphi')\rho' f(\varphi)^2\sec^2\varphi'\, d\rho' d\varphi'$$

$$+ \int\int \frac{jke^{-jk\sqrt{\sum_n^{x,y,z}\left(\widehat{u_n}\rho' f(\varphi') + \widehat{v_n}\,\rho' f(\varphi')\tan\varphi' - h\widehat{h_n}\right)^2}}}{4\pi\sum_n^{x,y,z}\left(\widehat{u_n}\rho' f(\varphi') + \widehat{v_n}\,\rho' f(\varphi')\tan\varphi' - h\widehat{h_n}\right)^2} * \begin{bmatrix} \widehat{u_x}\rho' f(\varphi') \\ +\widehat{v_x}\,\rho' f(\varphi')\tan\varphi' \\ -h\widehat{h_x} \end{bmatrix} N_{yz}(\rho',\varphi')\rho' f(\varphi)^2\sec^2\varphi'\, d\rho' d\varphi' \quad (2.9)$$

Since the second integral in eqn. (2.9) was weakly singular in its original form, its singularity is cancelled by the polar transformation for $h = 0$ ($\rho'$ terms cancel). The $\sec^2\varphi'$ in the numerator diverges at the same time and rate as the $\tan^2\varphi'$ in the denominator as $\varphi'$ approaches an odd multiple of $\frac{\pi}{2}$, creating a limit equal to 1 for their quotient. Furthermore, $f(\varphi')$ and $f(\varphi')\tan\varphi'$ are always finite for a valid transformation, as is clear from eqn. (2.1), and the angular integrand will be shown below to be well-behaved under typical circumstances. As such, the second integral may be evaluated numerically using standard quadrature rules such as the well-known Gauss-Legendre method. The first integral, in fact, is also regular despite the integrand's $\rho' = 0, h = 0$ singularity, but the justification of this claim is more involved. To show that the first integral is regular, we will examine its behavior as $\rho' \to 0$ for $h = 0$ (the observation point is in the source domain). When $h = 0$, the first eqn. (2.9) integral simplifies to the following expression:

$$\int \frac{\int I_x(\rho',\varphi')\, d\varphi'}{4\pi\rho'} d\rho', \quad (2.10)$$

with

$$I_x(\rho',\varphi') \equiv \operatorname{sgn}(\cos\varphi') \frac{e^{-jk\rho' f(\varphi')\sqrt{\sum_n^{x,y,z}(\widehat{u_n} + \widehat{v_n}\tan\varphi')^2}}}{\left[\sum_n^{x,y,z}(\widehat{u_n} + \widehat{v_n}\tan\varphi')^2\right]^{\frac{3}{2}}} * \{\left[\widehat{u_x} + \widehat{v_x}\tan\varphi'\right]N_{yz}(\rho',\varphi')\}\sec^2\varphi'. \quad (2.11)$$

Note that the cancellations from the simplification yield an expression that includes sgn(f($\varphi'$). Here, we have replaced the signum argument with $\cos\varphi'$ since $\operatorname{sgn}(\cos\varphi')$ and sgn(f($\varphi'$) are equal. This is apparent by consulting Fig. 1. When $-\frac{\pi}{2} < \varphi' < \frac{\pi}{2}$, $u' > u_0$, so $\operatorname{sgn}\left(f(\varphi')\right)$ must be positive.

The opposite is true when $\frac{\pi}{2} < \varphi' < \frac{3\pi}{2}$.

From here, we wish to take the limit of eqn. (2.11) as $\rho' \to 0$, where the integrand appears to diverge. If the limit exists, however, the integral is regular. To prove that the limit is indeed finite, we notice that if $\lim_{\rho' \to 0} \int I(\rho', \varphi')\, d\varphi' = 0$, the $\rho'$ integrand in eqn. (2.10) is a L'Hopital indeterminant. When $\rho' = 0$, $I_x(\rho', \varphi')$ becomes

$$I_x(0, \varphi') = \frac{\operatorname{sgn}(\cos \varphi')}{\left[\sum_n^{x,y,z} (\widehat{u_n} + \widehat{v_n} \tan \varphi')^2\right]^{\frac{3}{2}}} * [\widehat{u_x} + \widehat{v_x} \tan \varphi'] N_{yz}(0) \sec^2 \varphi'. \quad (2.12)$$

Note that when $\rho' = 0$, $N_{yz}$ is no longer a function of $\varphi'$. We now represent the numerator integral of eqn. (2.11), in a principal value sense, as follows:

$$\int_0^{2\pi} I_x(0, \varphi') d\varphi' = \lim_{\epsilon \to 0} \int_{-\frac{\pi}{2}+\epsilon}^{\frac{\pi}{2}-\epsilon} I_x(0, \varphi') d\varphi' + \int_{\frac{\pi}{2}+\epsilon}^{\frac{3\pi}{2}-\epsilon} I_x(0, \varphi') d\varphi'. \quad (2.13)$$

The bounds are chosen to coincide with the divergent points in the tangent and secant functions in the integrand. Using the same tangent-secant limit arguments as those used for the second integral of eqn. (2.9), we see that $I(0, \varphi')$ does not diverge at the integral bounds as $\epsilon \to 0$. Also note that for the first integral in eqn. (2.13), $\operatorname{sgn}(\cos \varphi') = 1$, whereas $\operatorname{sgn}(\cos \varphi') = -1$ in the second integral. We also notice that for $\varphi' \neq \frac{p\pi}{2}$ for some odd integer $p$,

$$\tan(\varphi' + \pi) = \tan \varphi', \quad (2.14a)$$

$$\sec^2(\varphi' + \pi) = \sec^2 \varphi'. \quad (2.14b)$$

Since the intervals of the two integrals in eqn. (2.13) are offset by $\pi$, it is clear that

$$\left| \lim_{\epsilon \to 0} \int_{-\frac{\pi}{2}+\epsilon}^{\frac{\pi}{2}-\epsilon} I_x(0, \varphi') d\varphi' \right| = \left| \lim_{\epsilon \to 0} \int_{\frac{\pi}{2}+\epsilon}^{\frac{3\pi}{2}-\epsilon} I_x(0, \varphi') d\varphi' \right|. \quad (2.15)$$

Therefore,

$$\lim_{\epsilon \to 0} \int_{-\frac{\pi}{2}+\epsilon}^{\frac{\pi}{2}-\epsilon} I_x(0, \varphi') d\varphi' + \int_{\frac{\pi}{2}+\epsilon}^{\frac{3\pi}{2}-\epsilon} I_x(0, \varphi') d\varphi' = \lim_{\epsilon \to 0} \int_{-\frac{\pi}{2}+\epsilon}^{\frac{\pi}{2}-\epsilon} I_x(0, \varphi') d\varphi' - \int_{-\frac{\pi}{2}+\epsilon}^{\frac{\pi}{2}-\epsilon} I_x(0, \varphi') d\varphi' = 0. \quad (2.16)$$

The limit in eqn. (2.10), then, is indeed a L'Hopital indeterminant, and thus may be evaluated via L'Hopital's rule. Differentiating the numerator and denominator of eqn. (2.10) with respect to $\rho'$, we can take the limit of eqn. (2.10) as follows:

$$\lim_{\rho' \to 0} \frac{\int I_x(\rho', \varphi')\, d\varphi'}{4\pi\rho'} = \frac{1}{4\pi} \int -jkf(\varphi') \sqrt{\sum_n^{x,y,z} (\widehat{u_n} + \widehat{v_n} \tan \varphi')^2}\ I_x(0, \varphi') d\varphi', \quad (2.17)$$

which is a regular integral that may be evaluated normally. This analysis shows that the polar mapping defined in eqn. (2.1) reveals that the strong singularity of the Helmholtz integral is a "false" singularity, one that does not truly cause the integrand to diverge. As such, both integrals of eqn. (2.9) may be evaluated numerically, using conventional quadrature rules without the need for singularity extraction. In fact, examining eqn. (2.9), we find that the limit integral in eqn. (2.17), when $\rho' = 0$, is exactly equal to the second $\varphi'$ integral in eqn. (2.9) in magnitude and opposite in sign. This means that at the $\rho' = 0$ point, the total integrand is null, i.e., the $\rho' = 0$ point contributes nothing to the integral. This is also trivially true if $\rho' = 0$ and $h \neq 0$. Identical arguments may be made to evaluate the second and third terms of eqn. (2.5). Note that the transformation described in this section is applicable to any 2D planar shape. This is a powerful result since, as far as 2D planar shapes are concerned, it allows for a one-size-fits-all technique for the numerical integration of the integral under consideration herein. It should be noted that weakly singular $1/R$ Helmholtz integrals also have their singularities cancelled with this transformation, much like the second integral in eqn. (2.9). This means that the formulation is also open to problems involving $1/R$ potential integrals. In the next section, we will explain the method of moving the polygon definition to the $(u, v)$ space.

## III. $(u, v)$ Transformation

Consider a polygon defined in Cartesian space by $N$ arbitrary points $\overrightarrow{x_1}$, $\overrightarrow{x_2}$, … and $\overrightarrow{x_n}$ defined as

$$\overrightarrow{x_n} = (x_{nx},\ x_{ny},\ x_{nz}),\ n = 1, 2, \ldots N. \quad (3.1)$$

We will execute an unscaled change of basis to represent the points within the polygon in terms of two orthogonal vectors that are in-plane with the polygon surface. The exact choice of basis is somewhat arbitrary, and many definitions are available. Here, we will choose the unit vector pointing from the polygon centroid $\vec{c}$ to the vertex $\overrightarrow{x_2}$ as our first basis

vector, which will establish the $\hat{v}$ direction (note, as shown in Fig. 1, the convention for this work is to label the lower left vertex of the polygon as $\overrightarrow{x_1}$ and increase the vertex numbering in the clockwise direction). $\vec{c}$ may be easily computed as

$$\vec{c} = \frac{1}{N}\begin{bmatrix} \sum_{n=1}^{N} x_{nx}\,, \\ \sum_{n=1}^{N} x_{ny}\,, \\ \sum_{n=1}^{N} x_{nz} \end{bmatrix}. \tag{3.2}$$

With this convention, $\hat{v}$ may be explicitly computed as

$$\hat{v} = \frac{\overrightarrow{x_2} - \vec{c}}{|\overrightarrow{x_2} - \vec{c}|}. \tag{3.3}$$

Using the unit vector pointing from $\overrightarrow{x_1}$ to $\overrightarrow{x_2}$, which we will label as $\widehat{l_{21}}$, we may develop an orthogonal vector to $\hat{v}$, which we will term $\hat{u}$:

$$\hat{u} = \frac{\hat{v} \times \widehat{l_{21}} \times \hat{v}}{\left|\hat{v} \times \widehat{l_{21}} \times \hat{v}\right|} = \frac{\widehat{l_{21}} - \hat{v}\left(\hat{v} \cdot \widehat{l_{21}}\right)}{\left|\widehat{l_{21}} - \hat{v}\left(\hat{v} \cdot \widehat{l_{21}}\right)\right|}, \tag{3.4}$$

where the BAC-CAB vector triple product identity has been used. Note that any in-plane vector that is not parallel to $\hat{v}$ may be used in place of $\widehat{l_{21}}$ and the resulting vector will be the same after normalization. We now represent each point within the polygon via the following function:

$$\overrightarrow{x'} = \vec{c} + u'\hat{u} + v'\hat{v}, \tag{3.5}$$

where $u'$ and $v'$ are constants. To find the constants that correspond to the point of interest $\overrightarrow{x'}$, we use individual components of eqn. (2.5) to create a system of equations, which may be represented in matrix form as below:

$$\begin{bmatrix} \widehat{u_x} & \widehat{v_x} \\ \widehat{u_y} & \widehat{v_y} \end{bmatrix}\begin{bmatrix} u' \\ v' \end{bmatrix} = \begin{bmatrix} \left(\overrightarrow{x'} - \vec{c}\right)_x \\ \left(\overrightarrow{x'} - \vec{c}\right)_y \end{bmatrix}. \tag{3.6}$$

Solving this matrix equation yields the unknown constants. Note that since all the points in the polygon are coplanar, each pair of two components can only correspond to one potential third coordinate while remaining in-plane, so only two of the components of eqn. (3.4) need to be invoked to find the unknown constants (here the $x$ and $y$ components are used). Note also that our differential element $dS'$ is now $du'dv'$. Since the Euclidean distances between points in our new basis and the original Cartesian basis are identical, no scaling factors are needed to execute the change of variables. We are now prepared to execute the polar mapping for polygons. This will be done in the next section.

## IV. Polygon Polar Coordinates

Here, we will demonstrate an example of how to execute the polar mapping described in the previous sections for arbitrary polygons with straight edges. The polar coordinates $\rho'$ and $\varphi'$ are defined in relation to the point $(u_0, v_0)$ and the polygon vertices. From Fig. 1, it is clear that $\varphi'$ is defined by the direction of the vector pointing from $(u_0, v_0)$ to $(u', v')$. $\rho'$, in our formulation, will refer to an inner polygon scaling factor that corresponds to the dimensions of a similar polygon to the polygon under consideration (note that the term "similar" is meant in the mathematical geometric sense). This similar polygon will be termed the "scaled" polygon. The scaled polygon has an edge that intersects with $(u', v')$ and vertices that lie on the lines drawn between $(u_0, v_0)$ and the vertices of the larger polygon, which we will term the "base" polygon. Fig. 2 illustrates this scaling concept. When $\rho' = 1$, $(u', v')$ lies on the base polygon boundary. We now define vertex vectors:

$$\overrightarrow{w_n} = \overrightarrow{p_n} - (u_0, v_0), \quad n = 1, 2, \ldots N. \tag{4.1}$$

where $\overrightarrow{p_n}$ denotes the $(u, v)$ coordinates of vertex n. These vectors will be used to determine the scaling of the similar polygon, and thus, $\rho'$. For some $(u', v')$ that we wish to map, we first must determine which edge the similar polygon will intersect the point with. We may do this by simply computing $\varphi'$ via

$$\varphi' = \tan^{-1}\frac{v' - v_0}{u' - u_0}. \tag{4.2}$$

We also define vertex $\varphi'$ values as

$$\varphi'_n = \tan^{-1}\frac{\overrightarrow{w_{nv}}}{\overrightarrow{w_{nu}}}, \quad n = 1, 2, \ldots N. \tag{4.3}$$

If $\varphi'_{n+1} \leq \varphi' < \varphi'_n$ the point is on edge $e_{(n+1)n}$. We will term the edge that corresponds to the $\varphi'$ value as the "active" edge. Note that if $(u_0, v_0)$ lies on a vertex, one of the vertex vectors will be 0 and its inverse tangent computation will be undefined. If $\varphi'$ is within an interval with an undefined bound, this undefined bound is replaced by the next defined bound in the sequence counting down from N to 1 and circling back to N.

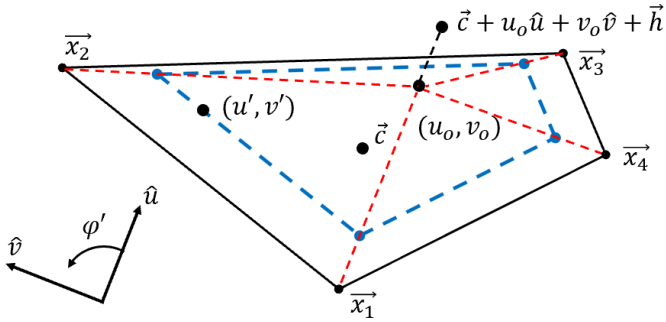


Fig. 2. Polygon scaling. The black polygon is the base polygon and the dashed blue polygon is the scaled polygon. The scaled polygon vertices lie on the red dashed lines connecting $(u_0, v_0)$ to the base polygon vertices and the scaled polygon edges are parallel to the base polygon edges. $(u', v')$ lies on a scaled polygon edge and $\rho'$ is determined by how large the scaled polygon must be for its boundary to intersect with $(u', v')$.

For example, for $N = 3$, if the undefined bound is $\varphi'_3$, we set $\varphi'_3 = \varphi'_2$ instead. If the undefined bound is $\varphi'_2$, we set $\varphi'_2 = \varphi'_1$. Finally, if the undefined bound is $\varphi'_1$, we set $\varphi'_1 = \varphi'_3$. This effectively merges two potential active edges together. As we will see below, both of the merged active edges are treated identically regarding the numerical integration operation. Once the active edge is known, we may use the vertex vectors to determine the intersection.

For a straight edge $e_{ij}$, let

$$(u', v') = (u_0, v_0) + \rho'\overrightarrow{w_j} + \beta\rho'\left(\overrightarrow{w_i} - \overrightarrow{w_j}\right), \tag{4.4}$$

and let

$$\overrightarrow{w_{ij}} = \overrightarrow{w_i} - \overrightarrow{w_j}, \tag{4.5}$$

where $\beta$ is some constant. Note that the *i-j* indexing assumes clockwise vertex increment, so starting at vertex 1 for $N = 3$, the edges are $e_{21}$, $e_{32}$, and $e_{13}$. Qualitatively, this operation shifts the observation point to the j[th] vertex of the scaled polygon that intersects with the source point and then moves along $e_{ij}$ of the scaled polygon until the source point is reached. This gives us two equations, one composed of $u$ coordinates and one composed of $v$ coordinates. By substitution, it is straightforward to eliminate $\beta$ and show that

$$\rho' = \frac{\overrightarrow{w_{iju}}(v' - v_0) - \overrightarrow{w_{ijv}}(u' - u_0)}{\overrightarrow{w_{jv}}\overrightarrow{w_{iju}} - \overrightarrow{w_{ju}}\overrightarrow{w_{ijv}}}, \tag{4.6}$$

where the $u$ and $v$ subscripts denote the $u$ and $v$ components of the vectors. Note that when $\rho' = 1$, the source point always lies on the polygon periphery. Using eqn. (4.2), we may represent $u'$ in terms of $\rho'$ as

$$u' = \rho' \frac{\overrightarrow{w_{jv}}\overrightarrow{w_{iju}} - \overrightarrow{w_{ju}}\overrightarrow{w_{ijv}}}{\overrightarrow{w_{iju}}\tan\varphi' - \overrightarrow{w_{ijv}}} + u_0. \tag{4.7}$$

From our definition in eqn. (2.1), this implies the azimuth function $f(\varphi')$ is

$$f(\varphi') = \frac{\overrightarrow{w_{jv}}\overrightarrow{w_{iju}} - \overrightarrow{w_{ju}}\overrightarrow{w_{ijv}}}{\overrightarrow{w_{iju}}\tan\varphi' - \overrightarrow{w_{ijv}}}. \tag{4.8}$$

This function encodes the varying Euclidean distance between $(u_0, v_0)$ and the source point as the scaled polygon edge is traversed, allowing for the transformation to be standardized across all polygon shapes under a single formulation. While we are effectively breaking the polygon into *N* sub-triangles, similarly to other polar formulations, it is the consideration of each scaled polygon as its own unified shape with constant "radius" $\rho'$ that differentiates the proposed scheme. This thinking ultimately facilitates 0 to $2\pi$ angular extent crucial to the proof of convergent exact strong singularity presented in the previous section. As we will see, the azimuth function combined with the rest of the integrands of the scaled polar formulation exhibit an angular dependence that is smooth enough to be tractable using Gaussian quadrature rules for the $\varphi'$ integration. The number of necessary sample points will be discussed in Section VI.

An aspect of this technique that should be noted is what happens if the observation point $(u_0, v_0)$ lies on an edge or vertex of the base polygon. If this is the case and $\varphi'$ is such that the active edge of the scaled polygon overlaps entirely with the base polygon boundary, $\overrightarrow{w_{jv}}\overrightarrow{w_{iju}} = \overrightarrow{w_{ju}}\overrightarrow{w_{ijv}}$ for all $\varphi'$ in that interval, and thus, $(u', v') = (u_0, v_0)$ since $f(\varphi') = 0$. To show that this is the case, consider $(u_0, v_0)$ lying on an arbitrary edge/vertex. Again, if this is the case, then every point on one or two of the scaled polygon edges (one if the source point is on a base polygon edge and not a vertex, and two if it's on a vertex) lies on the base polygon boundary. Let $e_{ijb}$ be the base polygon edge that overlaps with one of the scaled polygon edges. Given the overlap, it is clear that $\overrightarrow{e_{ijb}} \times \overrightarrow{w_i} = \overrightarrow{e_{ijb}} \times \overrightarrow{w_j} = 0$ (note $\overrightarrow{e_{ijb}}$ is the vector between vertex $i$ and vertex $j$). Therefore, we may state that for some constant $\alpha$, $\overrightarrow{w_i} = \alpha\overrightarrow{w_j}$, meaning that $\overrightarrow{w_{ij}} = (\alpha - 1)\overrightarrow{w_j}$. Since $(\alpha - 1)$ is scalar, it is clear then that $\overrightarrow{w_{jv}}\overrightarrow{w_{iju}} = \overrightarrow{w_{ju}}\overrightarrow{w_{ijv}}$ for this case. However, $\rho'$ is not necessarily equal to 0, depending on the size of the scaled polygon under consideration. Note that eqn. (4.6) cannot be used in this case to determine $\rho'$ since direct evaluation yields an indeterminant. Since our objective is numerical integration, however, we may simply assert $\rho'$ values during the evaluation process, so the potential ambiguity is not a problem.

In any case, a $f(\varphi')$ equal to 0 does not change the analysis (it merely causes the integrand exponential and the $\rho' = 0$ limit integrand to vanish), and thus, edge/vertex observation points do not require special treatment other than the active edge merging described above if the observation point is a vertex.

This now constitutes everything needed to evaluate the strongly singular integral over an arbitrary polygon. In the following sections, we will discuss some near-singularity strategies and show example computations of the eqn. (2.5) integral using the above formulation.

## V. Near-Singularity Treatment

For the above formulation, special care must be taken if the observation point is close to the source domain, but not lying exactly on it, thus creating a near-singularity. Under this circumstance, the integral computation becomes unwieldy near the projected observation point, and a spiked delta function-type behavior is observed, similar to the phenomenon highlighted in [5] that motivates focused treatment of near-singular cases. During our analysis, this was empirically found to occur, with varying intensities, when the length of the vector connecting the observation point and its projection is between ~$10^{-20}$ and $10^{-1}$. Below this range, the principal value behavior begins to dominate, and the integrand spike is suppressed. Above it, the spike fails to develop appreciably. To deal with the spike, if the length of the projection distance

vector, $|\vec{h}|$, is within this range, we break the radial integral into several logarithmic $\rho'$ intervals. The first interval is [0, $10|\vec{h}|$], the second is from [$10|\vec{h}|$, $100|\vec{h}|$], and so on until $10^N|\vec{h}|$ exceeds 0.1. Then, the rest of the integral is computed on the interval [$10^N|\vec{h}|$, 1]. This is similar in style to the "$h$-refinement" technique discussed in [5], only involving far fewer sample points. The distance from $\rho' = 0$ that the spike's maximum value occurs is proportional to $|\vec{h}|$, and this interval technique was empirically found to capture the dynamics of the spike well. Smaller interval divisions are possible, but were not found to increase evaluation accuracy substantially. The $\rho'$ integral on each interval is computed using the above formulation and Gaussian quadrature rules, as reducing the interval size creates smooth integrands in $\rho'$. In this way, the scaled polar formulation may be used in a general manner, even when near-singularities are involved. In the next section, we will demonstrate the results when applying this technique to a triangular domain.

## VI. Numerical Example

To demonstrate polar regularization integrand computation, we will consider a triangular integration domain along with associated RWG basis functions [10]. These basis functions are defined for triangle pairs where one edge is shared between the triangles. As described in [10], for each shared edge, one triangle is the "+" triangle and one is the "–" triangle. Here, we will consider all of the edges of both triangles to be interior to the greater domain that the triangles are partially discretizing, meaning that there are three basis functions to evaluate (see eqn. (9) of [10]). Consider a + triangle with vertices $\overrightarrow{x_1}$, $\overrightarrow{x_2}$, and $\overrightarrow{x_3}$ in Cartesian coordinates as before. Similarly to above, we may form edge vectors defined as

$$\overrightarrow{l_{21}} = \overrightarrow{x_2} - \overrightarrow{x_1}, \tag{5.1a}$$

$$\overrightarrow{l_{32}} = \overrightarrow{x_3} - \overrightarrow{x_2}, \tag{5.1b}$$

$$\overrightarrow{l_{13}} = \overrightarrow{x_1} - \overrightarrow{x_3}, \tag{5.1c}$$

and compute the triangle area as

$$A = \frac{1}{2}\left|\overrightarrow{l_{13}} \times \overrightarrow{l_{21}}\right|. \tag{5.2}$$

From here, we define the three RWG basis functions as

$$\vec{\boldsymbol{N}}_{\boldsymbol{1}}(\overrightarrow{x'}) = \frac{\left|\overrightarrow{l_{32}}\right|}{2A}\left(\overrightarrow{x'} - \overrightarrow{x_1}\right), \tag{5.3a}$$

$$\vec{\boldsymbol{N}}_{\boldsymbol{2}}(\overrightarrow{x'}) = \frac{\left|\overrightarrow{l_{13}}\right|}{2A}\left(\overrightarrow{x'} - \overrightarrow{x_2}\right), \tag{5.3b}$$

$$\vec{\boldsymbol{N}}_{\boldsymbol{3}}(\overrightarrow{x'}) = \frac{\left|\overrightarrow{l_{21}}\right|}{2A}\left(\overrightarrow{x'} - \overrightarrow{x_3}\right), \tag{5.3c}$$

where some $\overrightarrow{x'}$ lies within the triangle. The – triangle is formed by introducing a 4th node $\overrightarrow{x_4}$, establishing $e_{32}$ as the shared edge, and developing the – triangle basis functions accordingly. For the – triangle, $\vec{\boldsymbol{N}}_{\boldsymbol{1}}(\overrightarrow{x'})$ corresponds to the $\overrightarrow{x_4}$ node. With these basis functions, we may now evaluate eqn. (2.5). As shown in the previous sections, this integral, once transformed, consists of a double integral in $\rho'$-$\varphi'$ space. Since the integral is regular, as proved previously, it may be evaluated using one's desired choice of quadrature rules. Here, for demonstrative purposes, we will evaluate the $\varphi'$ integral first and plot the resulting $\rho'$ integrand as a function of $\rho'$ to show that it is finite and continuous when $\rho' = 0$. That is, we may represent the integral we wish to evaluate as

$$\int_0^1 \int_0^{2\pi} I'(\rho', \varphi') d\varphi' d\rho', \tag{5.4}$$

and we will plot the function

$$g(\rho') = \int_0^{2\pi} I'(\rho', \varphi') d\varphi' \tag{5.5}$$

to show integrand existence and continuity for all $\rho'$ values. Note that $I'(\rho', \varphi')$ may be found by following procedures similar to those outlined in eqns. (2.5)-(2.9), only for all the terms in the eqn. (2.5) brackets. We will choose a randomly-generated set of nodes for this exercise with vertices defined as follows:

$$\overrightarrow{x_1} = [-.0276, \quad .0042, \quad .0246], \tag{5.6a}$$

$$\overrightarrow{x_2} = [.0012, \quad -.0349, \quad .0294], \tag{5.6b}$$

$$\overrightarrow{x_3} = [-.0251, \quad .0188, \quad .0343], \tag{5.6c}$$

$$\overrightarrow{x_4} = [.0291, \quad -.0050, \quad .0099]. \tag{5.6d}$$

Note that the vertices have been scaled such that the maximum triangle side-length is equal to λ/10 at 500 MHz. The shared edge for the triangle pair will be that connecting $\overrightarrow{x_2}$ and $\overrightarrow{x_3}$, with $\overrightarrow{x_1}$ belonging only to the + triangle and $\overrightarrow{x_4}$ belonging to the – triangle. Following the polar regularization procedures described above, we obtain the integrand functions shown in Figs. 3, 4 for the + and – triangle $\vec{\boldsymbol{N}}_{\boldsymbol{1}}(\overrightarrow{x'})$ basis functions when the observation point is placed in the center of the shared edge, which we will term $\overrightarrow{m_{32}}$, and offset by with a vector equal to $10^{-3}$ times the vector connecting $\overrightarrow{m_{32}}$ and the + triangle centroid, giving an $|\vec{h}|$ of $3.6938 \times 10^{-6}$ for the – triangle (the observation point is still within the + triangle, so $|\vec{h}| = 0$ for that one) with $\hat{h} = -.6583\hat{x} - .2578\hat{y} - .7072\hat{z}$. As demonstrated by the plots in Fig. 5, the $\rho'$ integrands for an observation point lying on the source domain are indeed smooth and continuous for all values of $\rho'$ including $\rho' = 0$,

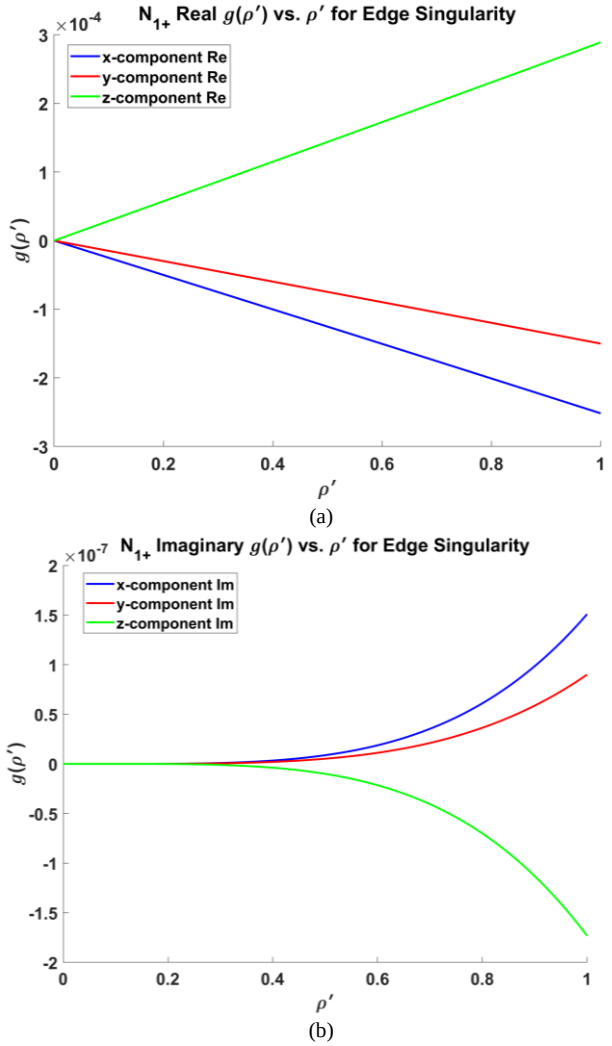


Fig. 3. λ/10 + triangle $\vec{N}_1(\vec{x'})$ $\rho'$ integrand real part (a) and imaginary part (b).

where the integrand vanishes. In fact, the real parts are linear in nature for small triangles, which is an advantageous property, as it lowers the required number of sample points for accurate integration.

For the – triangle, the observation point position corresponds to 6 interval separations given our logarithmic interval scaling. Fig. 4 shows the $\vec{N}_1(\vec{x'})$ $g(\rho')$ values computed for the – triangle for $\rho' = [0, 1]$, with a zoomed-in plot showing the $\rho' = [0, 10|\vec{h}|]$ interval for the real part. As is apparent from the figure, significant spikes in the integrand functions present themselves for this case, the spike peaks are adequately smooth within the first interval choice. The remaining intervals ensure that the fall-off from the large spike values is effectively represented. For all of these plots, the $g(\rho')$ values were computed using Gaussian quadrature rules with 11 sample points per active edge (33 points in total for the angular integral). This confirms that the integrals are tractable under the polar transformation.

To examine the convergence dynamics, we plot the asymptotic behavior of the integral evaluations as the number of Gaussian quadrature sample points is increased. This will be done for

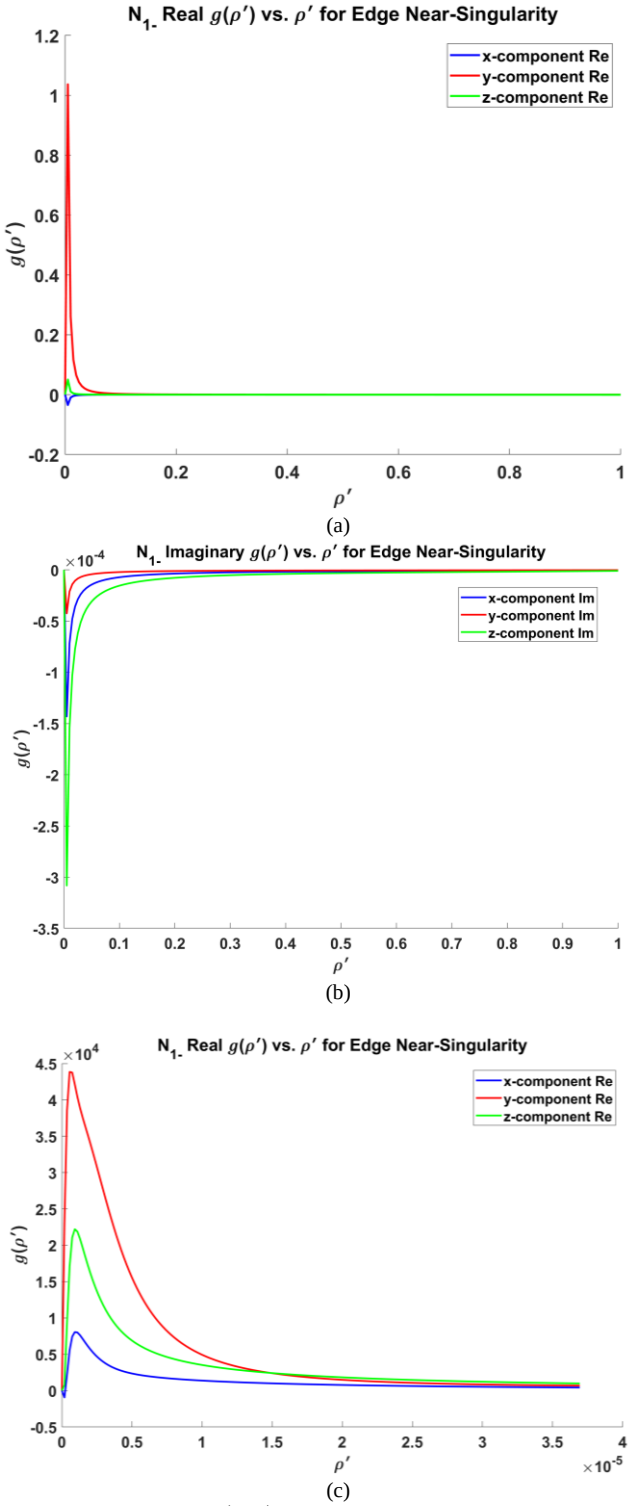


Fig. 4. λ/10 – triangle $\vec{N}_1(\vec{x'})$ $\rho'$ integrand real part (a) and imaginary part (b), with zoomed-in view of near-singular spike (c).

the observation point just described. For simplicity, we will keep the number of sample points the same for both the angular and radial integrals, though this is not required. Figs. 5, 6 demonstrate the convergence for the $\vec{N}_1(\vec{x'})$ basis function. The plots show the absolute value of the difference between the integrals evaluated using differing numbers of sample points and the integrals evaluated using 101 sample

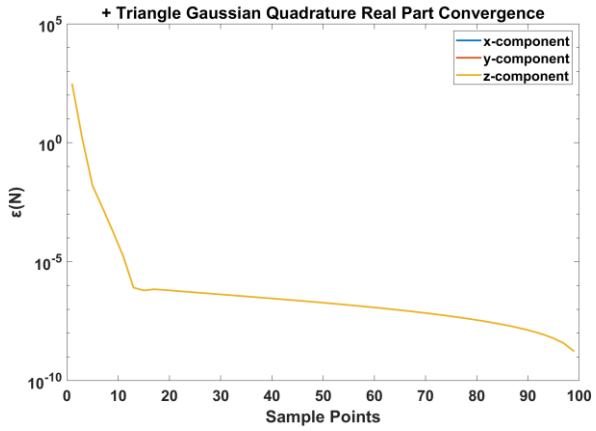


(a)

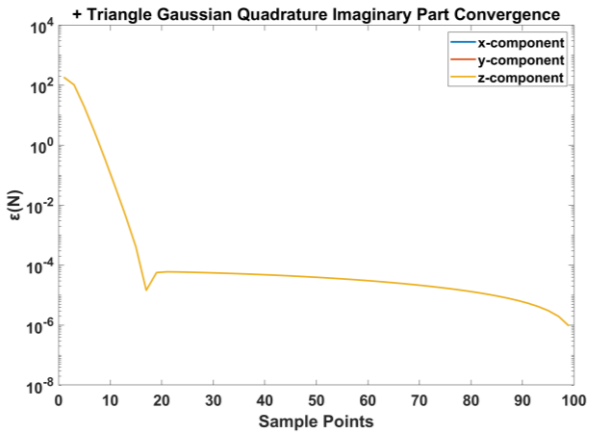


(b)

Fig. 5. λ/10 + triangle $\vec{N}_1(\vec{x'})$ Gaussian quadrature convergence.

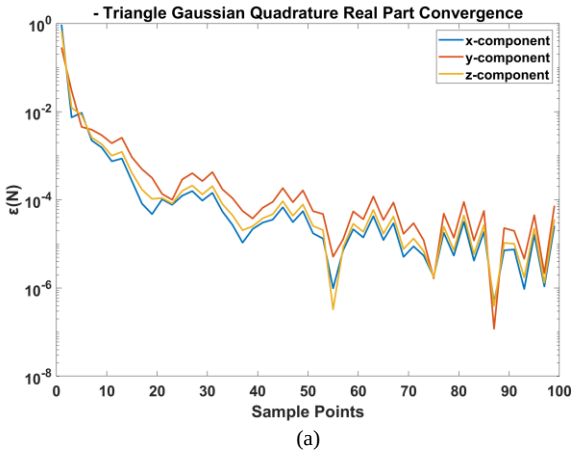


(a)

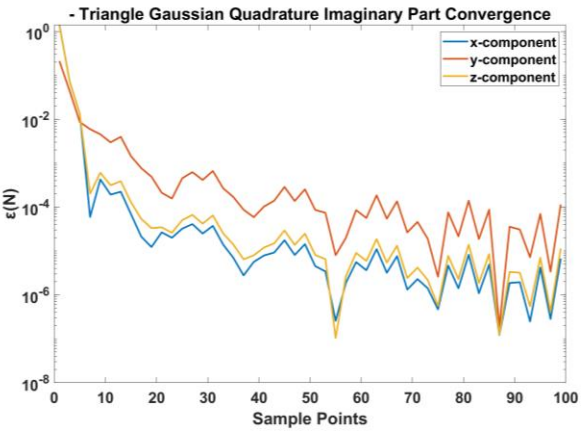


(b)

Fig. 6. λ/10 – triangle $\vec{N}_1(\vec{x'})$ Gaussian quadrature convergence with 6 interval separations for $|\vec{h}|$ of $3.6938 \times 10^{-6}$.

points, normalized by the 101 sample point integral. Note this is done for each vector component. That is, we plot the value $\varepsilon$ defined as

$$\varepsilon(N) = \frac{|I_N - I_{101}|}{|I_{101}|}, \tag{5.7}$$

where $I_N$ is a component of the real or imaginary part of the integral evaluation using $N$ sample points and $I_{101}$ is the evaluation of that component for 101 sample points. Note the total number of Gaussian quadrature evaluations for both the angular and radial integrals is $3N^2$ for the + triangle and $18N^2$ for the – triangle since 6 intervals are used for the near-singularity. For the + triangle evaluations, which contain the observation points in their source domains, the convergence requires ~20 or more sample points to achieve precision on the order of $1 \times 10^{-6}$ for the real part and $1 \times 10^{-4}$ for the imaginary part (all components have the same convergence behavior, so their curves overlap). Note that for these calculations, the imaginary part is several orders of magnitude smaller than the real part, which impacts the relative precision. The convergence on the – triangle is more modest, with a less stable precision curve that is below $1 \times 10^{-3}$ for 20 or more sample points for both the real and imaginary parts. This is expected, since these integrals deal with the near-singularities. It should be noted that the precision is impacted negatively by the size of the triangle and the direction of the projection vector from the triangle domain to the near-singularity. To show this, we will repeat the convergence exercise for the same triangles scaled to λ/5 instead of λ/10, and place the observation point at a position that is offset from the center of the shared edge by λ/100 in the direction perpendicular to the + triangle plane, similarly to a case examined in [9]. The results are shown in Figs. 7, 8. As the plots demonstrate, the + triangle precision is greatly improved, achieving results similar to previous works ([6]-[9]), while the precision for the – triangle is largely unchanged. Since the previous works in the literature, to the author's knowledge, only demonstrate near-singularities with purely perpendicular projections, it is unclear how other methods would compare regarding the non-perpendicular projections and small triangles examined here. Nevertheless, the technique provided here is fully-numerical, natively supports any basis function, can be used on planar polygons with an arbitrary number of edges, and is directly applicable to strong and weak singularities alike. Because of this, and because even the reduced precision results are sufficient for most applications, the method proposed in this work shows great usefulness. In Table 1, for completeness, we show the total integral evaluations, taken to four significant digits, for each basis function for the λ/10 triangles and the first

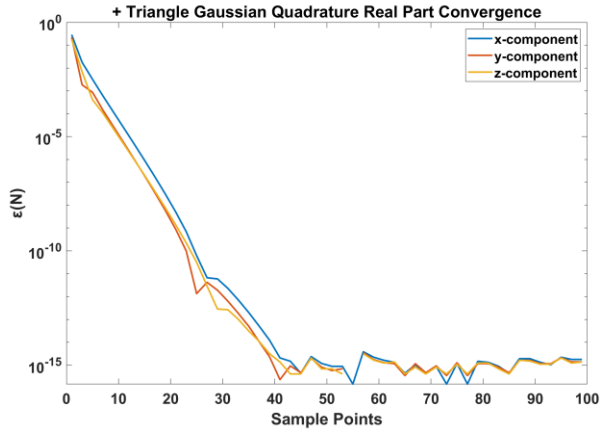


(a)

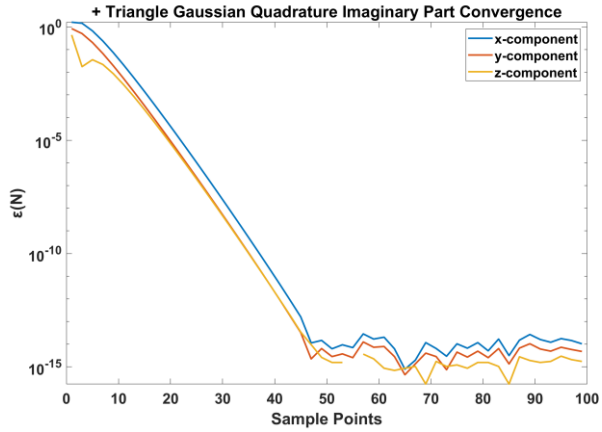


(b)

Fig. 6. λ/5, +-triangle-perpendicular observation point + triangle $\vec{N}_1(\vec{x'})$ Gaussian quadrature convergence with 3 interval separations for $|\vec{h}|$ of .006. The breaks in the curve represent points where the reference and test integrals are equal to machine precision.

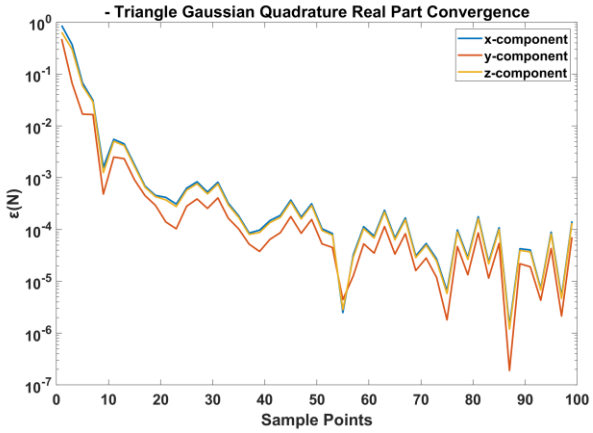


(a)

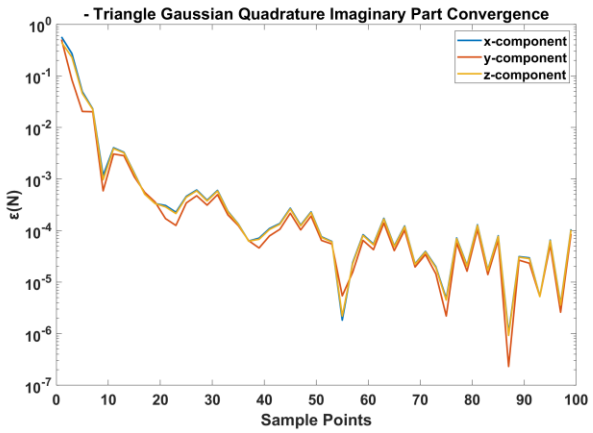


(b)

Fig. 7. λ/5, +-triangle-perpendicular observation point – triangle $\vec{N}_1(\vec{x'})$ Gaussian quadrature convergence with 3 interval separations for $|\vec{h}|$ of .006.

observation point described above. Recall that this observation point is exactly singular for the + triangle and near-singular for the – triangle.

## VII. Conclusion

In this work, we have demonstrated a polar transformation technique that regularizes the strong singularity found in common Helmholtz surface integrals used in MoM formulations regardless of observation point position. The technique is applicable to any basis function and straight-edged planar shape, making it highly versatile compared to singularity extraction techniques, which require a new analytical integral to be evaluated for each type of shape and basis function. Moreover, the polar scaling formalism is intrinsically open to extension to higher order surfaces and more sophisticated edge geometries (as opposed to simple straight edges). These topics will be the focus of future research. Furthermore, this work rigorously proves that the Helmholtz strongly singular integral is convergent, whereas no such proof has been made readily available in the literature for this case before now. The technique of this work has been shown to smoothly regularize the integrand such that the latter may be simply evaluated with Gaussian quadrature rules.

TABLE I
Polar Regularized Singular and Near-Singular Integral Results

| Basis Function | + | – |
|---|---|---|
| $\vec{N}_1(\vec{x'})$ | $10^{-4}$ $\times[(-1.254+.0003j)\hat{x}$ $+(-.7475+.0002j)\hat{y}$ $+(1.439-.0004j)\hat{z}$ | $[(.0567-.0000j)\hat{x}$ $+(.2691-.0000j)\hat{y}$ $+(.1527-.0000j)\hat{z}$ |
| $\vec{N}_2(\vec{x'})$ | $10^{-4}$ $\times[(2.432-.1485j)\hat{x}$ $+(1.450-.0886j)\hat{y}$ $+(-2.792+.1705j)\hat{z}$ | $[(.3563+.0001i)\hat{x}$ $+(.0138+.0000j)\hat{y}$ $+(.2095+.0003j)\hat{z}$ |
| $\vec{N}_3(\vec{x'})$ | $10^{-4}$ $\times[(-5.673+.4086j)\hat{x}$ $+(-3.382+.2436j)\hat{y}$ $+(6.513+.4691j)\hat{z}$ | $[(-.2930-.0001j)\hat{x}$ $+(-.2185-.0000j)\hat{y}$ $+(-.2649-.0002j)\hat{z}$ |

As such, the technique proposed here represents a powerful method for evaluating Helmholtz integrals over planar domains.

## References

[1] R. D. Graglia, "On the numerical integration of the linear shape functions times the 3-D Green's function or its gradient on a plane triangle," in *IEEE Transactions on Antennas and Propagation*, vol. 41, no. 10, pp. 1448-1455, Oct. 1993, doi: 10.1109/8.247786.

[2] Ilari Hanninen, Matti Taskinen, and Jukka Sarvas, "Singularity Subtraction Integral Formulae for Surface Integral Equations with RWG, Rooftop and Hybrid Basis Functions," in *Progress In Electromagnetics Research*, Vol. 63, 243-278, 2006. doi:10.2528/PIER06051901.

[3] P.W. Fink, D. R.Wilton, and M. A. Khayat, "Issues and methods concerning the evaluation of hypersingular and near-hypersingular integrals in BEM formulations," presented at the Int. Conf. Electromagnetics in Advanced Applications, Torino, Italy, Sep. 2005.

[4] F. Vipiana and D. R. Wilton, "Numerical Evaluation via Singularity Cancellation Schemes of Near-Singular Integrals Involving the Gradient of Helmholtz-Type Potentials," in *IEEE Transactions on Antennas and Propagation*, vol. 61, no. 3, pp. 1255-1265, March 2013, doi: 10.1109/TAP.2012.2227922.

[5] P. W. Fink, D. R. Wilton and M. A. Khayat, "Simple and Efficient Numerical Evaluation of Near-Hypersingular Integrals," in *IEEE Antennas and Wireless Propagation Letters*, vol. 7, pp. 469-472, 2008, doi: 10.1109/LAWP.2008.2000788.

[6] M. -D. Zhu, T. K. Sarkar, Y. Zhang and M. Salazar-Palma, "A Novel Framework of Singularity Cancellation Transformations for Strongly Near-Singular Integrals," in *IEEE Transactions on Antennas and Propagation*, vol. 69, no. 12, pp. 8539-8550, Dec. 2021, doi: 10.1109/TAP.2021.3083834.

[7] Ismatullah and T. F. Eibert, "Adaptive Singularity Cancellation for Efficient Treatment of Near-Singular and Near-Hypersingular Integrals in Surface Integral Equation Formulations," in *IEEE Transactions on Antennas and Propagation*, vol. 56, no. 1, pp. 274-278, Jan. 2008, doi: 10.1109/TAP.2007.913170.

[8] M. G. Duffy, "Quadrature over a pyramid or cube of integrands with a singularity at a vertex," *SIAM J. Numer. Anal.*, vol. 19, no. 6, pp.1260–1262, 1982.

[9] J. Rivero, F. Vipiana, D. R. Wilton and W. A. Johnson, "Hybrid Integration Scheme for the Evaluation of Strongly Singular and Near-Singular Integrals in Surface Integral Equations," in *IEEE Transactions on Antennas and Propagation*, vol. 67, no. 10, pp. 6532-6540, Oct. 2019, doi: 10.1109/TAP.2019.2920333.

[10] S. M. Rao, D. R. Wilton, and A. W. Glisson, "Electromagnetic scattering by surfaces of arbitrary shape," *IEEE Trans. Antennas Propag.*, vol. AP-30, no. 3, pp. 409–418, May 1982.